Wuhan University
Journal of Natural Sciences

2016, Vol.21 No.4, 358-368

Article ID 1007-1202(2016)04-0358-11
DOI 10.1007/s11859-016-1182-5

Spatial and Temporal Variability of $PM_{2.5}$ Concentration in China

□ XU Gang, JIAO Limin†, ZHAO Suli, CHENG Jiaqi

School of Resource and Environmental Sciences, Wuhan University, Wuhan 430079, Hubei, China

Abstract: $PM_{2.5}$ has become an increasing public concern recently because of its visibility reduction and severe health risks. For the whole year of 2013, hourly $PM_{2.5}$ data of 496 monitoring sites scattered in 74 cities of China are collected to analyze temporal and spatial variability of $PM_{2.5}$ concentration. Different temporal scales (seasonal variation, monthly variation and daily variation) and spatial scales (urban versus rural, typical areas and national scale) are discussed. Results show that $PM_{2.5}$ concentration changes significantly in both long-term and short-term scales. An apparent bimodal pattern exists in daily variation of $PM_{2.5}$ concentration and the daytime peak appears around 10:00 am while the lowest concentration appears around 16:00 pm. Spatial autocorrelation analysis and Ordinary Kriging are used to characterize spatial variability. Moran's I of $PM_{2.5}$ concentration in three typical regions, the Beijing-Tianjin-Hebei region, the Yangtze River Delta region and the Pearl River Delta region, is 0.906, 0.693, 0.746, respectively, which indicates that $PM_{2.5}$ is strong spatial correlated. Spatial distribution of annual $PM_{2.5}$ concentration simulated by Ordinary Kriging shows that 7.94 million km^2 (83%) areas fail in meeting the requirement of China's National Ambient Air Quality Standards Level-2 (35 $\mu g/m^3$) and there are at least three concentrated highly polluted areas across the country.

Key words: air pollution; $PM_{2.5}$; spatial-temporal variability; spatial autocorrelation

CLC number: X 513, P 951

Received date: 2015-06-16

Foundation item: Supported by the National Natural Science Foundation of China (41571385).

Biography: XU Gang, male, Ph.D. candidate, research direction: air pollution geo-science modeling. E-mail: xugang@whu.edu.cn

†To whom correspondence should be addressed. E-mail: lmjiao027@163.com

0 Introduction

No one can doubt China's remarkable economic achievements in the past three decades. Although a great deal of efforts in air pollution reduction has been made, China is still suffering from severe air pollution largely due to the rapid economic growth and high population density [1, 2]. Recently, $PM_{2.5}$ (particles with aerodynamic diameter less than 2.5 microns) has become a public concern because of its visibility reduction and severe health impacts. Numerous epidemiological studies demonstrate that respiratory and cardiovascular diseases are closely associated with $PM_{2.5}$ [3-5]. What's more, $PM_{2.5}$ has been the primary air pollutant in many Chinese cities [2].

As any other air pollutants, $PM_{2.5}$ concentration varies significantly whether at temporal scales or spatial scales. Imbalance of economic development and differences of geographical conditions lead to obvious regional disparity (large scale) of $PM_{2.5}$ pollution. In terms of city scale (small scale), $PM_{2.5}$ concentration also shows apparent spatial heterogeneity and temporal variability due to ① Uneven distribution of emission sources; ② Fluctuations of emissions; ③ Complexity of air dispersion condition [6, 7]. As spatial-temporal variability of $PM_{2.5}$ concentration is of significant importance for air quality monitoring, assessing and controlling, many previous spatial-temporal analyses have been conducted on city or regional scale. Russell *et al* [8] found out obvious seasonal variation of $PM_{2.5}$ concentration with higher concentration in late fall and pronounced morning peak in its daily variation in Southeast Texas. Strong seasonal and daily variations of $PM_{2.5}$ concentration have also

been identified in other areas [9, 10]. However, because of the limited extent representativeness and small numbers of monitoring sites, spatial characterization analysis is much more difficult than temporal variability analysis. Many methods, including spatial interpolation, Land Use Regression (LUR) and satellite-derived aerosol optical depth (AOD), are introduced for high spatial resolution simulation of $PM_{2.5}$ concentration at diverse scales from intra-city to globe [11-13]. As one of the most popular methods used for spatial interpolation, Kriging has been used in many disciplines, as well as in air pollution mapping and spatial variability analysis [14,15]. As other ecology phenomenon, the spatial distribution of $PM_{2.5}$ concentration is not independent but correlated with each other, which is called spatial autocorrelation. Spatial autocorrelation analysis was also used in some previous researches [16], but few are related to $PM_{2.5}$ pollution.

Although spatial or temporal variability of $PM_{2.5}$ or PM_{10} concentration was analyzed in some typical cites or regions in China [17, 18], this study focuses on $PM_{2.5}$ concentration variability at different temporal and spatial scales, especially in diverse aspects analysis of temporal variability. In this study, long-term variation (seasonal variation and monthly variation) and short-term variation (daily variation) of $PM_{2.5}$ concentration from three aspects (types of monitoring sites, north-south gap and regional disparity) will be characterized in Section 2.1 and Section 2.2. As for spatial variability, spatial autocorrelation analysis will be applied into three typical regions followed by $PM_{2.5}$ concentration spatial distribution simulation using Ordinary Kriging in Section 2.3 and Section 2.4. It is worth noting that spatial-temporal variability affects each other, for example, spatial variability of $PM_{2.5}$ concentration is also reflected in temporal variability analysis from diverse aspects.

1 Materials and Methods

1.1 $PM_{2.5}$ Data

The Ministry of Environmental Protection of China enacted new Ambient Air Quality Standards (GB3095 -2012) in February, 2012 and started $PM_{2.5}$ routine monitoring from December, 2012. The first batch of 496 monitoring sites in 74 cities are mainly located in three typical regions, the Beijing-Tianjin-Hebei (BTH) region, the Yangtze River Delta (YRD) region and the Pearl River Delta (PRD) region. Provincial capital cities and some other large cities are also included in the first batch. There are 10-15 monitoring sites in megacities, like Beijing and Shanghai, and 3-6 monitoring sites in other prefecture-level cities. Hourly $PM_{2.5}$ data of 496 monitoring sites for the whole year of 2013, excluding Taiwan, Hong Kong and Macao, were collected from China National Environmental Monitoring Center.

1.2 Temporal Variability

As for temporal variability, long-term variation (seasonal variation and monthly variation) and short-term variation (daily variation) of $PM_{2.5}$ concentration will be characterized. However, temporal variability differs from each other in various places on consequence of large areas of China. Three aspects will be considered when we analyze temporal variability.

1) Types of monitoring sites

Monitoring sites can be divided into two groups, urban-site and clean-site. Urban-sites are located in urban areas while clean-sites are located in suburban areas, usually in rural areas or nature protection areas. Clean-sites are used for representing the background concentration of air pollutants. There are differences between urban-sites and clean-sites, which reflects rural-urban disparity of $PM_{2.5}$ pollution. Not all cities have clean-site and there are only 38 clean-sites among 496 sites. The average distance between each clean-site and the nearest urban-site in the same city is 20.7 km for all 38 clean-sites.

2) North-south gap

Air pollution in northern China is much more serious than that in south. In addition to natural condition disparity between north and south, government-led heating operation exacerbates the severe air pollution in northern China in winter since coal burning for heating is the main source of air pollutants including $PM_{2.5}$. Because of obvious differences of $PM_{2.5}$ pollution in north and south, it is necessary to analyze temporal variability respectively. For the aspect of north-south gap, 496 monitoring sites are divided into two parts, namely sites in the north and sites in the south, according to the Qinling Mountains-Huai River Line.

For sites in northern China, temporal variability of heating season and non-heating season will be analyzed. Government-led heating is provided for all cities in winter in the north of Qinling Mountains-Huai River Line. However, duration of heating is different among cities. For example, heating duration in Beijing starts on November 15 and terminates on March 15 next year, a total

of 4 months. While in higher-latitude (Harbin), it lasts from November 1 to March 31 in the next year, about 5 months. For convenience, heating season is defined as November to March, and the rest of the year (from April to October) is non-heating season for sites in northern China in this study.

In southern China, precipitation is the most significant characteristic of seasonal change, based on which a year is divided into dry, wet and transition periods. The duration of each period is also different from city to city in southern China. Since most cities in southern China undergo rainy season (also called wet period) from May to August, while on the other hand, the corresponding season of dry period is winter. As a consequence, dry period is defined as the period from November to February in the next year, and wet period is from May to August, and the rest (March, April, September and October) is transition period.

Seasonal variation and daily variation of $PM_{2.5}$ concentration in both northern and southern China will be discussed in Section 2.1 and Section 2.2.

3) Regional disparity

There are obvious regional disparity and spatial clusters of $PM_{2.5}$ pollution level(average) in China. The monitoring sites are distributed in nine regions (Table 1).

Table 1 Provinces included in nine regions

Regions	Provinces included
North China	Beijing, Tianjin, Hebei, Shanxi, Inner Mongolia, Shandong
East China	Shanghai, Jiangsu, Zhejiang, Anhui
South China	Guangdong, Fujian
Southwest China	Yunnan, Guizhou, Guangxi
Central China	Henan, Shaanxi, Hubei, Hunan, Sichuan, Chongqing, Jiangxi
Northwest China	Gansu, Qinghai, Ningxia
Northeast China	Heilongjiang, Jilin, Liaoning
Xinjiang	Xinjiang
Tibet	Tibet

Geographical position of sites, administrative boundary and $PM_{2.5}$ pollution level are taken into consideration when dividing those regions. Division result differs from traditional geographical division of China in some parts. It is important to pay attention to the difference of North China and northern China defined in Section 1.2. The extent of North China is shown in Table 1, while northern China represents region in the north of Qinling Mountains-Huai River Line. The difference between South China and southern China is the same. Although there is only one city that has carried out $PM_{2.5}$ monitoring in both Xinjiang and Tibet respectively, they are divided into two regions because $PM_{2.5}$ concentration differs greatly from each other as Urumqi is surrounded by desert with high $PM_{2.5}$ concentration while Lhasa is located in plateau with clean air.

1.3 Spatial Autocorrelation

The basic hypothesis of classical statistics is that the samples are independent. It often cannot meet the requirement when samples are geo-referenced because they are associated with each other called spatial dependence. Spatial autocorrelation refers to the relationship between certain attribution of one geographical object and the same attribution of other objects in the same geographical space. It is based on the first law of geography, which is "Everything is related to everything else, but near things are more related than distant things"[19]. Spatial autocorrelation is usually used to identify spatial distribution pattern of some phenomena (air pollution) and its associated values (concentration).

Positive spatial autocorrelation indicates that neighboring values are similar while negative spatial autocorrelation indicates dissimilar values. Moran's I [20] statistic is the most commonly used measures of spatial autocorrelation and there are some other measures including Geary's C [21]. Global Moran's I statistics put forward by Cliff [22] is used to examine whether spatial autocorrelation exists or not but it cannot tell where exist spatial clusters. Therefore, Anselin put forward local Moran's I statistics [23].

The global Moran's I statistic is as follows:

$$I = \frac{n}{S_0} \frac{\sum_{i=1}^{n}\sum_{j=1}^{n} w_{i,j} z_i z_j}{\sum_{i=1}^{n} z_i^2} \tag{1}$$

where Z_i is the deviation of an attribute for feature i from its mean $(x_i - \overline{X})$, $w_{i,j}$ is the spatial weight between features i and j, n is equal to the total number of features, and S_0 is the aggregate of all the spatial weights:

$$S_0 = \sum_{i=1}^{n}\sum_{j=1}^{n} w_{i,j} \tag{2}$$

In general, the value of Moran's I varies between −1 and 1, representing negative and positive spatial autocorrelation, respectively. The absolute value is closer to zero, which represents the weaker spatial autocorrelation.

The local Moran's I statistic is given as

$$I_i = \frac{x_i - \overline{X}}{S_i^2} \sum_{j=1, j\neq i}^{n} w_{i,j}(x_i - \overline{X}) \tag{3}$$

where x_i is an attribute for feature j, $\bar{X}$ is the mean of the corresponding attribute, $w_{i,j}$ is the spatial weight between feature i and j, and

$$S_i^2 = \frac{\sum_{j=1, j\neq i}^{n} w_{i,j}}{n-1} \bar{X}^2 \quad (4)$$

Since spatial distribution of $PM_{2.5}$ emissions (factories, traffic, etc.) is agglomerated coupled with the interaction of air diffusion and regional transportation, $PM_{2.5}$ values are highly auto-correlated [24]. Owing to monitoring sites are points, spatial weight matrix will be created using distance weight (Euclidean Distance) in GeoDA1.4.0. Results will be displayed using ArcGIS10.0.

As what mentioned before, monitoring sites are largely located in three typical regions, the BTH region, the YRD region and the PRD region, partly corresponding to North China, East China and South China. Spatial autocorrelation analysis will be applied in these three representative regions, not in the whole country. Other four cities (Jinan, Qingdao, Taiyuan and Hohhot) are added in the BTH region. Fuzhou, Xiamen and Haikou are excluded due to their large distances from the YRD region, although those three cities are included in South China area for regional temporal variability analysis.

1.4 Ordinary Kriging

Geostatistics refers to techniques used for mapping of surfaces from limited sample data and the estimation of values at unsampled locations. As one of the most popularly used methods, Kriging was first developed by Matheron [25] from an idea of Krige [26] and it was first used in mineral industry. Recently, Kriging has been widely used in many other fields including air pollution mapping [27, 28]. Kriging estimation is a three stages process: ① Estimation of the semi-variogram; ② Fitting the semi-variogram; ③ Punctual Kriging [14]. Firstly, semi-variogram $\gamma(\ )$ is used to characterize the spatial correlation of monitoring data as follows:

$$\gamma(h) = \frac{1}{2N(h)} \sum_{i=1}^{N(h)} [Z(S_i) - Z(S_i + h)]^2 \quad (5)$$

where h is the distance between two monitoring sites and $N(h)$ is the number of pairs with the same distance h. Secondly, three frequently referenced spatial models (spherical, exponential and Gaussian) are used to obtain the optimal semi-variogram parameters (range, partial sill and nugget) [29]. Finally, values at those unobserved locations will be estimated. As for the basic technique, Ordinary Kriging uses a weighted average of observed neighboring values to estimate the unobserved values at a given location as follows:

$$Z(S) = \sum_{i=1}^{N} \lambda_i Z(S_i) \quad (6)$$

where λ_i is calculated by introducing a Lagrange multiplier μ and solving the system:

$$\sum_{i=1}^{n} \lambda_i \gamma(h_{i,j}) + \mu = \gamma(h_{j,0}) \quad (7)$$

Under the constraint:

$$\sum_{i=1}^{N} \lambda_i = 1$$

where S is the predictive position; $Z(S)$ is the predictive value of point without observation; $Z(S_i)$ is the measurement of position i; λ_i is the weight of $Z(S_i)$ and N is number of measurement. The process will be carried out using Geostatistics Analyst in ArcGIS10.0 and as a result, spatial distribution of $PM_{2.5}$ concentration will be simulated.

2 Results

2.1 Long-Term Variation of $PM_{2.5}$ Concentration

1) Seasonal variation

For each site, daily averages are calculated from hourly monitoring results and then daily averages are used to obtain monthly averages. Seasonal averages of each site are calculated by averaging the aggregate of monthly averages. Ordinary season divisions in China are as follows: spring (March, April, May), summer (June, July, August), autumn (September, October, November) and winter (December, January, February). A year is divided according to ordinary season divisions when we analyze seasonal variation across China and in diverse regions. Distinguishing seasonal variation between northern China and southern China, a year is divided into heating season and non-heating season in northern China while it is divided into dry, wet and transient periods in southern China. Division methods in detail are described in Section 1.2. Table 2 shows the descriptive statistics of seasonal average $PM_{2.5}$ concentration of each site across China.

Average $PM_{2.5}$ concentration is 73.2 μg/m^3 aggregated from all 496 monitoring sites for the whole year of 2013, which exceeds twice of China's National Ambient Air Quality Standards Level-2 (35 μg/m^3). Seasonal averages of $PM_{2.5}$ concentration vary greatly from 44.9 μg/m^3 in summer to 113.7 μg/m^3 in winter and the later is 2.5 times of the former. Apparent seasonal differences

Table 2 Descriptive statistics of seasonal average $PM_{2.5}$ concentration

$\mu g \cdot m^{-3}$

Season	Min	Max	Median	Mean	S.D.
Spring	15.3	120.3	60.3	62.4	19.8
Summer	8.3	119.3	40.0	44.9	21.7
Autumn	16.3	174.3	65.3	68.8	26.1
Winter	19.3	288.9	111.7	113.7	48.4
Full year	16.4	164.9	72.4	73.2	26.1

exist in $PM_{2.5}$ concentration and $PM_{2.5}$ pollution level in winter is much more severe than that in the other three seasons. Influenced by monsoon climate, large parts of China features have a warm, rainy summer and a cold, dry winter.

The reasons that $PM_{2.5}$ concentration in winter is much higher than in summer can be summarized as the following three points: ① Particulate matter deposits and diffuses more easily in summer due to abundant rainfall and strong air convection, while in winter, due to low temperature, the downdrafts dominate which leads to insufficient air diffusion; ② Boundary layer height is much higher in summer, particulate matters have much range of motion with the same mass leading lower mass concentration in the ground level in summer; ③ Coal combustion in winter generates more air pollutants, especially in the north of China[3]. And coal burning in heating season puts great pressure on air quality in northern China and brings big gap of air pollution between north and south. Seasonal characteristics of $PM_{2.5}$ concentration in northern China and southern China are shown as Table 3.

Table 3 Seasonal characteristics (mean±S.D.) of $PM_{2.5}$ concentration in northern China and southern China

$\mu g \cdot m^{-3}$

Site type	Northern China		Southern China		
	Heating season	Non-heating season	Dry period	Wet period	Transient period
Urban-site	116.0±56.5	66.7±30.2	91.1±40.4	37.5±15.6	59.1±23.1
Clean-site	96.1±52.3	53.1±27.3	70.0±35.8	30.7±15.1	53.3±25.5
All sites	114.5±56.4	65.8±30.2	89.5±40.4	37.0±15.7	58.7±23.3

Table 3 shows that northern China has undergone severe $PM_{2.5}$ pollution. Even in non-heating season, the average $PM_{2.5}$ concentration of clean-site is 53.1 $\mu g/m^3$, which is more than 50% higher than National Ambient Air Quality Standards Level-2 (35 $\mu g/m^3$). Nevertheless, $PM_{2.5}$ pollution is much more serious in heating season. In 2013, $PM_{2.5}$ concentrations at urban-site and clean-site in heating season are 73.9% and 81.0% higher than that in non-heating season, respectively.

In heating season, $PM_{2.5}$ concentration of urban-site in northern China city is 19.9 $\mu g/m^3$ (20.7%, relatively) higher than that of clean-site. Correspondingly, in non-heating season, $PM_{2.5}$ concentration of urban-site in northern China city is 13.6 $\mu g/m^3$ (25.6%, relatively) higher than that of clean-site.

$PM_{2.5}$ pollution in southern China also shows significant seasonal differences. $PM_{2.5}$ concentration of dry period of all monitoring sites in southern China is 2.4 times higher than that of wet period, and it is also more than 50% higher than that of transition period.

As for disparity of pollution level between urban-site and clean-site, in dry period, $PM_{2.5}$ concentration of urban-site is 21.1 $\mu g/m^3$ higher than that of clean-site, while in wet and transient period, $PM_{2.5}$ concentrations of urban-site are 6.8 $\mu g/m^3$ and 5.8 $\mu g/m^3$ higher than that of clean-site, respectively. In dry, wet and transient period, $PM_{2.5}$ concentrations of urban-site are 30.1%, 22.1%, 10.9% relatively higher than that of clean-site.

Seasonal characteristics of $PM_{2.5}$ concentration in those 9 regions (Table 1) are summarized in Table 4, which combines all urban-sites and clean-sites. As for average $PM_{2.5}$ concentration, only Tibet meets the guidelines of National Ambient Air Quality Standards Level-2 (35 $\mu g/m^3$). It shows obvious air pollution disparity among different regions.

Air pollution is the most serious in North China with mean 90.3 $\mu g/m^3$ and is relatively mild in South China and Southwest China. As for seasonal variation, air quality is the cleanest in summer while it is polluted most in winter. $PM_{2.5}$ concentration in autumn is higher than in spring in 7 regions excluding Northwest China and Tibet.

2) Monthly variation

Monthly variations of $PM_{2.5}$ concentration at urban-sites and clean-sites of all sites being monitored are shown in Fig. 1. The error bars are the standard deviation of $PM_{2.5}$ concentration of urban-sites.

It is obvious that $PM_{2.5}$ concentration in clean-sites is lower than that in urban-sites and the trend of monthly

Table 4 Seasonal characteristics (mean±S.D.) of $PM_{2.5}$ concentration in 9 different regions

Region	Cities	Sites	$PM_{2.5}$ concentration / μg · m^{-3}				
			Spring	Summer	Autumn	Winter	Average
North China	17	114	78.4±69.2	72.8±62.1	87.2±80.1	133.2±126.4	90.3±87.9
East China	26	139	61.8±43.9	42.9±38.3	62.3±46.7	111.3±85.5	66.8±59.4
South China	12	71	41.0±28.8	21.7±17.1	49.4±29.0	62.0±44.9	42.7±34.1
Southwest China	3	25	48.3±29.5	25.7±17.0	52.8±33.6	66.2±46.0	47.1±35.3
Central China	7	76	76.6±50.4	46.0±33.3	83.0±59.5	138.6±100.4	83.8±71.6
Northwest China	3	15	62.3±71.9	38.9±49.4	54.2±63.5	75.8±56.3	56.5±62.3
Northeast China	4	43	52.0±46.2	37.4±36.1	67.9±90.2	110.6±98.9	65.1±76.8
Xinjiang	1	7	60.6±49.3	48.4±45.6	85.8±75.2	156.5±106.9	87.8±84.0
Tibet	1	6	26.1±19.8	19.7±19.5	21.5±18.7	28.9±35.5	23.8±23.9
All regions	74	496	62.4	44.9	68.8	113.7	73.2

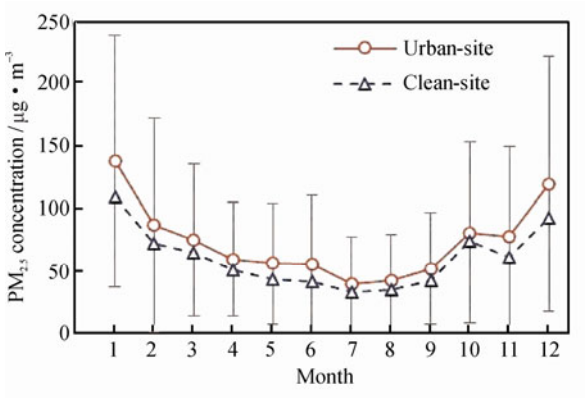

Fig. 1 Monthly variations of $PM_{2.5}$ concentration of urban-sites and clean-sites

variations of both types are consistent. However, as for monthly averages, the gap between two kinds of sites varies from 6.8 μg/m^3 in October, the smallest, to 29.2 μg/m^3 in January, the largest. The proportion of $PM_{2.5}$ concentration of clean-sites to urban-sites varies from 77.1% to 91.5% in each month. Another interesting point showed by Fig. 1 is that $PM_{2.5}$ concentration increases dramatically from September to October and then decreases from October to November. Gehrig and Buchmann [6] pointed out that it is meteorological effects that affect the monthly variation. In the future, more scientific analysis can be conducted to illustrate the interesting phenomenon.

Owing to the geographical differences and large regional disparity of $PM_{2.5}$ pollution in China, temporal variability of $PM_{2.5}$ concentration differs greatly. Monthly variations of $PM_{2.5}$ concentration averaged from all sites cannot reflect the differences among diverse regions. Therefore, monthly average $PM_{2.5}$ concentrations of 9 regions (Table 1) are calculated respectively. In order to compare the monthly variations of different regions, $PM_{2.5}$ concentration is 0-1 standardized for each region and the result is presented in Fig. 2. Types of monitoring sites are not distinguished, because we emphsize regional differences this time.

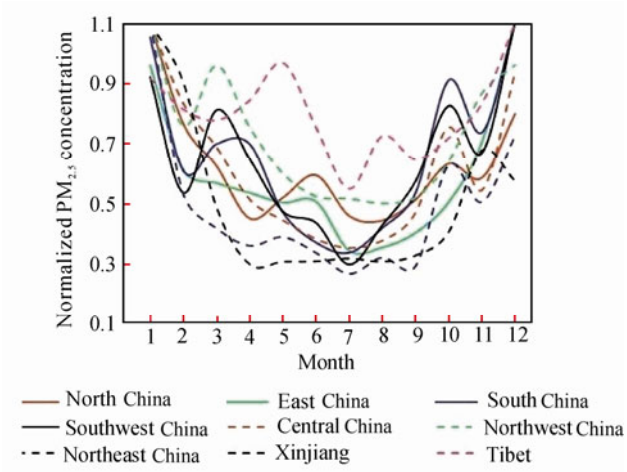

Fig. 2 Monthly variations of $PM_{2.5}$ concentration in 9 different regions of China

As it can be seen, monthly averages vary greatly among different regions differentiating from variations shown in Fig. 1. Two important differences should be noticed. First, $PM_{2.5}$ increased apparently after the decrease in late winter in some areas. For example, there is a remarkable increase in spring in South China, Southwest China and Northwest China, and there is also a remarkable increase in early summer in North China and Tibet. Second, Fig. 1 shows that there is an obvious decrease in November after a significant increase in October for sites across the country. Those areas, North China, South China, Central China, Northeast China and Southwest China regions, share the same variation pattern and the pattern is delayed for a month in Xinjiang. However, in other areas including East China, Northwest China and Tibet, the pollutants have been increasing from summer to winter without any decrease. As previ-

ously demonstrated, meteorological data should be taken into consideration when explanations for those diverse variation patterns in future research are given.

2.2 Short-Term Variation of $PM_{2.5}$ Concentration

Hourly averages of $PM_{2.5}$ concentration are summarized every hour. A comparison of daily variations of $PM_{2.5}$ concentration between urban-site and clean-site is presented in Fig. 3. The error bars are one standard deviation of $PM_{2.5}$ concentration of urban-sites.

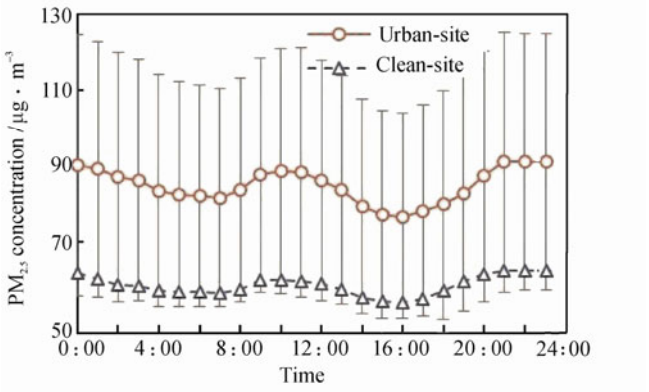

Fig. 3 Daily variations of $PM_{2.5}$ concentration of urban-sites and clean-sites

The same as monthly variation, variation tendency of daily variation of urban-site and clean-site is also highly consistent. Additionally, the gap between two kinds of site is apparent and $PM_{2.5}$ concentration of urban-site is 26.1 μg/m^3 higher than clean-site in average. However, the proportion of $PM_{2.5}$ concentration of clean-sites in urban-sites is pretty stable as it varies from 67.5% to 72.3% each hour. There is a distinct bimodal (double-peak) pattern of daily variation in both urban-site and clean-site, which has been found out in other studies as well [7, 17]. The morning maximum and the night maximum appear around 10:00 am and 22:00 pm, respectively. Correspondingly, the afternoon minimum and the early morning minimum occur at around 16:00 pm and 6:00 am. Daily variation of $PM_{2.5}$ concentration can be explained by traffic intensity and dynamics of atmosphere [9]. As for the morning maximum, several explanations are put forward by different studies including ① large amount of vehicle emissions; ② low mixing heights; ③ bursts of photochemical activity associated with sunrise; ④ increased secondary particle production [7, 9]. $PM_{2.5}$ concentration daily variation in heating and non-heating seasons in northern China and daily variation of dry, wet and transient periods in southern China are summarized from hourly monitoring data at the corresponding time (month) and place (north and south). The results are presented in Fig. 4 and Fig. 5.

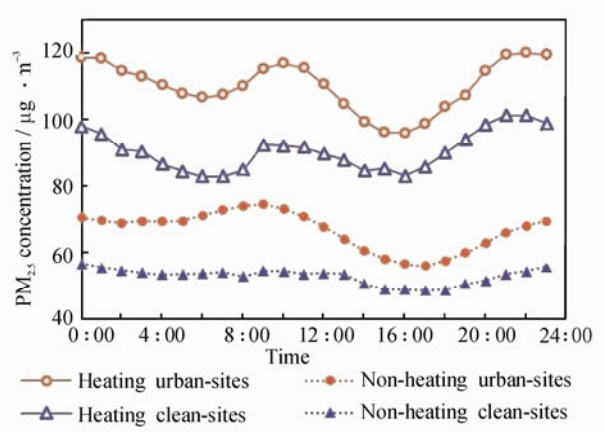

Fig. 4 Daily variation of $PM_{2.5}$ concentration of heating and non-heating seasons in northern China

Figure 4 shows that bimodal pattern also exists in $PM_{2.5}$ concentration daily variation in northern China. Overall, $PM_{2.5}$ concentration in heating season varies more greatly than that in non-heating season, while $PM_{2.5}$ concentration daily variation of urban-site fluctuates more greatly than that of clean-site. Bimodal patterns of urban-site and clean-site in heating season are apparent and so is daily variation of urban-site in non-heating season. By contrast, daily variation of clean-site in non-heating season is quite gentle. The former three that shows the most obvious daily variation reaches at peak at 9:00 am or 10:00 am, and falls to trough at 16:00 pm or 17:00 pm in the afternoon.

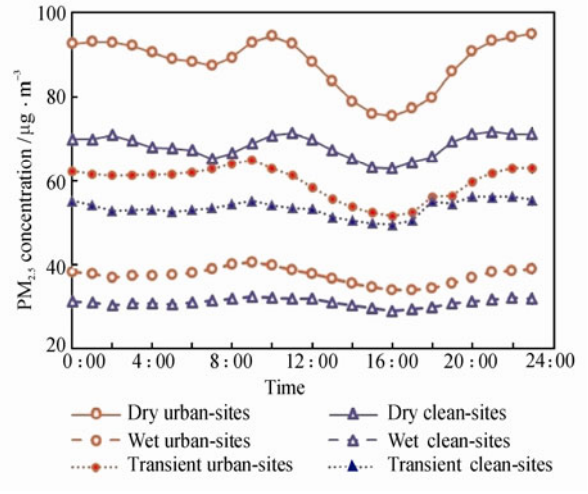

Fig. 5 Daily variation of $PM_{2.5}$ concentration of dry, wet and transient periods in southern China

In southern China, $PM_{2.5}$ concentration daily variation fluctuates in diverse degree among different periods and different monitoring site types. As a whole, $PM_{2.5}$ concentration daily variation in dry period fluctuates more greatly than that in wet period, while that in transient period varies between the two. As for different

monitoring site types, daily variation of urban-site varies more greatly than that at of clean-site, the same as in northern China. Consisting with Table 3, in dry period, the gap between urban-site and clean-site reaches the largest and the lowest in transient period. Moreover, $PM_{2.5}$ concentrations at urban-site and clean-site are similar at 18:00 pm in transition period. Daily variations of $PM_{2.5}$ concentration in 9 different regions are presented in Fig. 6.

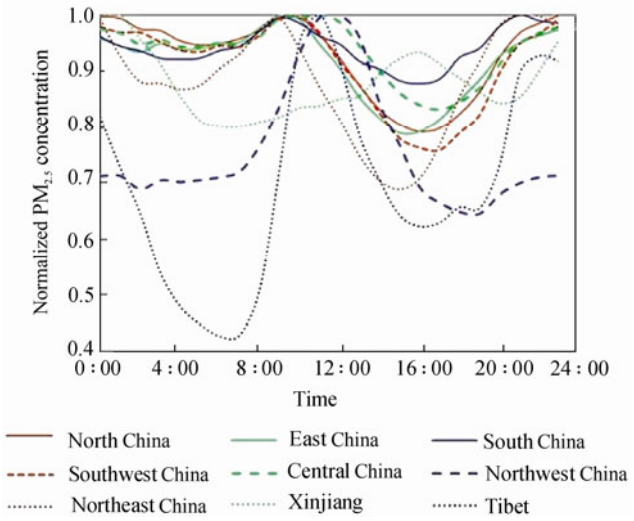

Fig. 6 Daily variations of $PM_{2.5}$ concentration in 9 different regions of China

Compared with monthly variation of $PM_{2.5}$ concentration, daily variations share great resemblance with bimodal pattern in different regions though extent of change varies greatly. Generally, change extent in daytime is greater than that at night except that in Tibet. For Northeast and Northwest China, there is also distinct valley at night resulting in a more obvious bimodal pattern. Moreover, $PM_{2.5}$ concentration is higher at night than that in daytime, but it is opposite in the northwest region of China and in Tibet. The peak in the morning appears at 9:00 am or 10:00 am and the trough in the afternoon appears from 15:00 pm to 17:00 pm. As for the appearance time of peak and trough, Xinjiang (Urumqi) differs from other regions and variation curve of Northwest China also translates 2-3 hours backward compared with other regions, since the monitoring time is Beijing time instead of local time and Xinjiang local time is 2 hours later than Beijing time.

2.3 Spatial Autocorrelation Analysis

As expected, $PM_{2.5}$ concentration is highly autocorrelated. Global Moran's I and local Moran's I are both employed to identify spatial autocorrelation of $PM_{2.5}$ concentration in three typical regions, the BTH region, the YRD region and the PRD region. Moran's I scatter plots of $PM_{2.5}$ concentrations in three typical regions using GeoDA are shown in Fig. 7.

Those 4 different quadrants of plots represent different types of spatial clusters. The first quadrant means High-High (H-H) cluster, that's to say, monitoring

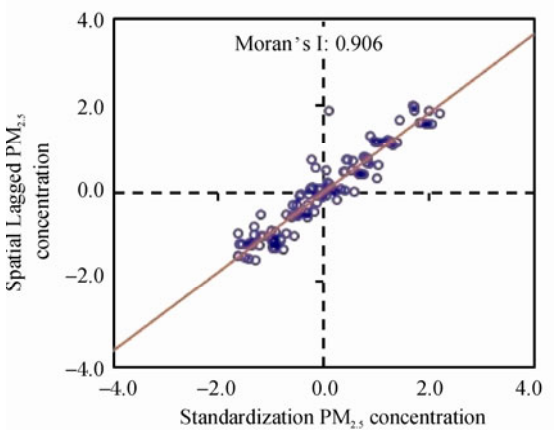

(a) The BTH region

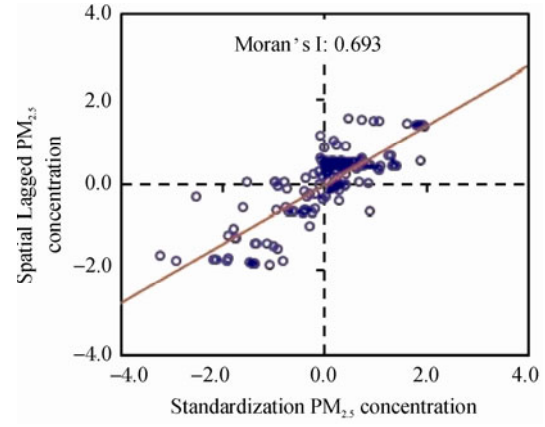

(b) The YRD region

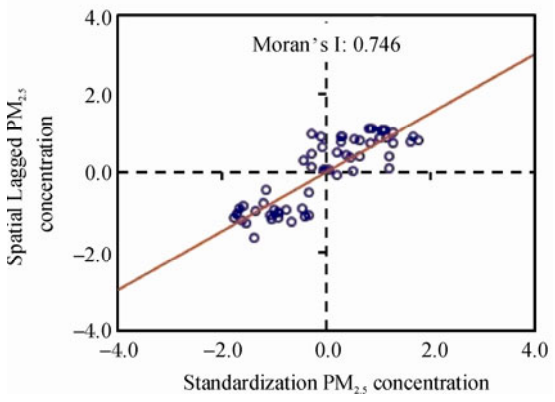

(c) The PRD region

Fig. 7 Moran's I scatter plots of $PM_{2.5}$ concentration

x-coordinate of plot is standardized $PM_{2.5}$ concentration; *y*-coordinate is spatial lagged $PM_{2.5}$ concentration determined by spatial weight matrix based on Euclidean distance between monitoring sites

sites with high $PM_{2.5}$ concentrations are also surrounded by sites with high values.

The second quadrant means Low-High (L-H) cluster, namely $PM_{2.5}$ concentration at one site is low but its surrounding concentration is higher. Similarly, the third and fourth quadrant means Low-Low (L-L) cluster and High-Low (H-L) cluster. H-H cluster and L-L cluster reflect the homogeneity of $PM_{2.5}$ pollution, which indicates positive spatial autocorrelation of $PM_{2.5}$ concentration among those sites. By contrast, L-H cluster and H-L cluster reflect the heterogeneity of $PM_{2.5}$ pollution, which indicates negative spatial autocorrelation.

Most monitoring sites in three typical regions are characterized as H-H cluster or L-L cluster, which illustrates strong spatial autocorrelation, which exists in all three regions with high Moran's I: 0.906 in the BTH region, 0.693 in the YRD region and 0.746 in the PRD region. At the same time, a few sites with strong spatial heterogeneity are shown as L-H cluster or H-L cluster. Scatter plot of BTH is the most linear centralized and most sites are characterized as H-H cluster or L-L cluster. YRD has the lowest Moron's I because most of the points are distributed around (0, 0), which indicates that spatial clusters of those sites may be non-significant.

Clusters of $PM_{2.5}$ pollution can be spatialized using local spatial autocorrelation analysis in GeoDA. Spatial pattern, as well as hotspots and cold spots of $PM_{2.5}$ pollution, can be identified in local spatial cluster map shown as Fig. 8. Across the BTH region, there is no obvious spatial cluster for sites in Beijing and Tianjin. Monitoring sites in South Hebei Province (Xingtai, Handan and Shijiazhuang) and Tangshan city are H-H clusters. Those cities are also the most polluted areas. On the other hand, sites in the other cities are L-L clusters.

As for the YRD region, two obvious differences exist in the local spatial cluster. One is the difference between south and north. The sites in the north of the region (most of the Jiangsu Province) are more likely to be hotspots while the sites in the south of the region (most of Zhejiang Province) are more likely to be cold spots. The other is with land-sea discrepancy that sites in coastal cities are tending to be cold spots and sites in inland cities are tending to be hotspots.

Compared with the other two regions, the distribution density of monitoring sites in the PRD region is the most reasonable. Land-sea contrast in this area is very obvious as sites near the sea are more likely to be cold spots while inland sites are more likely to be hotspots.

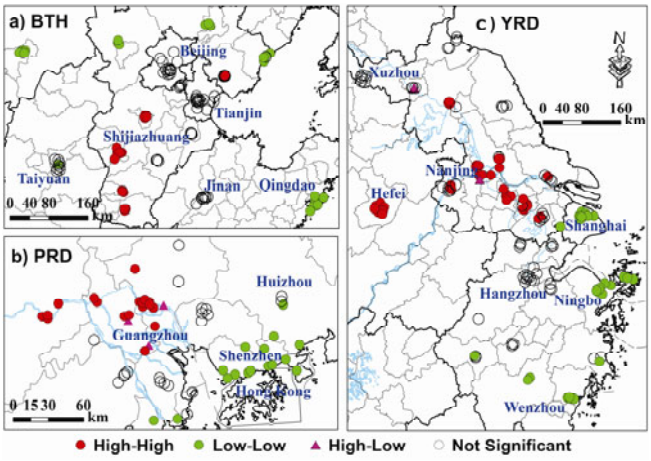

Fig. 8 Local spatial cluster map for $PM_{2.5}$ concentration

2.4 Spatial Distribution of $PM_{2.5}$ Concentration

Continuous spatial distribution of $PM_{2.5}$ concentration is very important for health impact assessment of $PM_{2.5}$ exposure and other purposes. However, sparse ground monitoring sites cannot meet the requirement. Many methods are adopted to simulate surface of $PM_{2.5}$ concentration. In this study, we present simple spatial pattern of $PM_{2.5}$ concentration in China and a Kriging interpolation is an easy way for our purpose. Therefore, spatial distribution of average $PM_{2.5}$ concentration in 2013 is simulated using Ordinary Kriging. Cross-validation (CV) is used to examine the performance of Ordinary Kriging.

Monitoring sites are divided into validation set (20%) and experimental set (80%) randomly. In order to acquire predicted $PM_{2.5}$ values for validation set sites, spatial distribution of $PM_{2.5}$ is simulated using Ordinary Kriging based on monitoring sites of experimental set. Predicted $PM_{2.5}$ values for locations of validation set sites will be compared with those measured $PM_{2.5}$ concentrations. Pearson correlation coefficient is used to examine the relationship between measured and predicted concentration of each site. Root Mean Squared Prediction Error (RMSPE) is also used to estimate prediction precision of Ordinary Kriging. The result of cross validation is shown in Fig. 9. The result of cross validation shows that Ordinary Kriging performs quite well as R^2 is 0.892 and RMSPE is 8.1 μg/m^3, which indicates that Ordinary Kriging can explain 89% spatial variability of $PM_{2.5}$ average concentration. However, the sites with lower concentration are likely to be overestimated while the sites with higher concentration are likely to be underestimated, since the slope of plot is less than 1.

There are numerous researches on spatial distribution of air pollutant, recently. Some studies using differ-

ent methods have been successfully applied for spatial distribution simulation of NO_2, PM_{10} and $PM_{2.5}$ [30, 31] in China. Ma *et al* [31] estimated ground-level $PM_{2.5}$ in China using satellite remote sensing as cross-validation R^2 is 0.64. Although model used here has relative high accuracy (R^2=0.89), $PM_{2.5}$ concentration is likely to be over

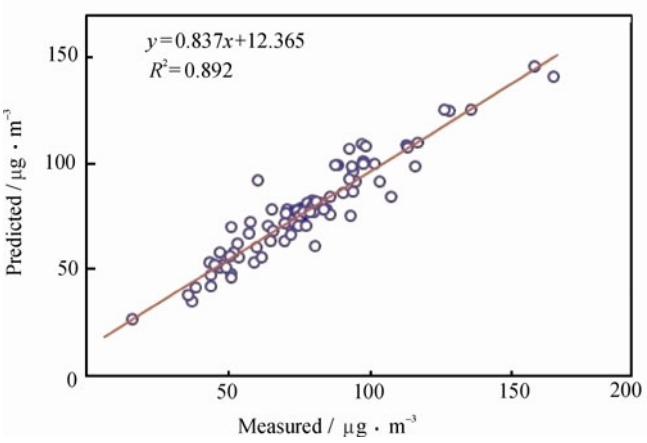

Fig. 9 Scatter plot between measured and predicted $PM_{2.5}$ concentration of validation set sites

estimated, especially for rural areas, because most of the monitoring sites are located in urban areas, by contrast, only 38 sites are situated in suburban or rural areas.

Due to the limited monitoring sites, especially in West China, all 496 monitoring sites are used to simulate the spatial distribution of $PM_{2.5}$ concentration. The result of Ordinary Kriging is shown only in areas covered by monitoring sites and experiencing severe $PM_{2.5}$ pollution in Fig. 10.

It is obvious that the situation of $PM_{2.5}$ pollution is much severe in most part of China. The contour line of 75 μg/m^3 is drawn and then areas of concentration

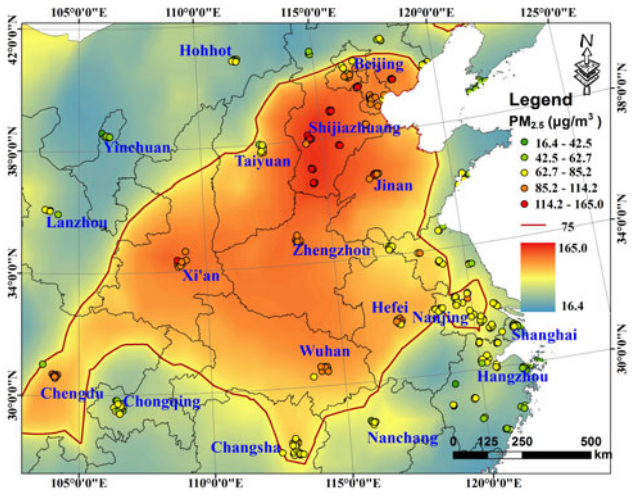

Fig. 10 Spatial distribution of average $PM_{2.5}$ concentration (2013)

exceeding 75 μg/m^3 are calculated in ArcGIS. There are at least three highly polluted areas which are circled by contour of 75 μg/m^3. The most conspicuous is North China, Central China and Southwest China concentrated pollution area with 1.22 million km^2 in total. Health impacts and economic loss of so serious $PM_{2.5}$ pollution are unimaginable since this region is one of the most densely populated areas in China. We also calculated areas in China where $PM_{2.5}$ concentration surpasses 35 μg/m^3 resulting in 7.94 million km^2, in other words, 83% of China fails in meeting the requirement of National Ambient Air Quality Standards Level-2 (35 μg/m^3).

3 Conclusion

1) In general, annual average $PM_{2.5}$ concentration in 2013 across China is 73.2 μg/m^3. 83% areas of China fail to meet the guidelines recommended by national Ambient Air Quality Standards (35 μg/m^3).

2) $PM_{2.5}$ concentration changes significantly in both long-term and short-term scales. $PM_{2.5}$ pollution level varies greatly in different seasons, especially between heating season and non-heating season in northern China. Monthly variation varies in different regions. However, daily variation shares the same bimodal pattern regardless of seasonal change and regional disparity. Throughout the day, $PM_{2.5}$ concentration is the highest around 10:00 am and lowest around 16:00 pm.

3) A strong spatial autocorrelation exists in three typical regions, the BTH, YRD and PRD regions, with high Moran's I：0.906, 0.693 and 0.746, respectively. Local spatial clusters for $PM_{2.5}$ concentration show that land-sea contrast has an obvious effect on $PM_{2.5}$ pollution. The spatial distribution by Ordinary Kriging displays that most parts of China suffer from severe $PM_{2.5}$ pollution, especially North and Central China, and there are at least three highly polluted areas. Result of cross-validation indicates that Ordinary Kriging can explain 89% spatial variability of $PM_{2.5}$ concentration.

References

[1] He K B, Huo H, Zhang Q. Urban air pollution in China: Current status, characteristics, and progress [J]. *Annual Review of Energy and the Environment*, 2002, **27**: 397-431.

[2] Chan C K, Yao X H. Air pollution in mega cities in China [J]. *Atmospheric Environment*, 2008, **42**(1): 1-42.

[3] Chen Y, Ebenstein A, Greenstone M, *et al*. Evidence on the impact of sustained exposure to air pollution on life

[4] expectancy from China's Huai River policy [J]. *Proc Natl Acad Sci USA*, 2013, **110**(32): 12936-12941.

[5] Zhang Y Q, He M Q, Wu S M, *et al*. Short-term effects of fine particulate matter and temperature on lung function among healthy college students in Wuhan, China[J]. *International Journal of Environmental Research and Public Health*, 2015,**12**(7):7777-7793.

[6] Brunekreef B, Holgate S T. Air pollution and health [J]. *The Lancet*, 2002, **360**(9341): 1233-1242.

[7] Gehrig R, Buchmann B. Characterising seasonal variations and spatial distribution of ambient PM_{10} and $PM_{2.5}$ concentrations based on long-term Swiss monitoring data [J]. *Atmospheric Environment*, 2003, **37**(19): 2571-2580.

[8] Xu G, Jiao L M, Zhao S, *et al.* Examining the impacts of land use on air quality from a spatio-temporal perspective in Wuhan, China [J]. *Atmosphere,* 2016, **7**(5): 62.

[9] Russell M, Allen D T, Collins D R, *et al.* Daily, seasonal and spatial trends in $PM_{2.5}$ mass and composition in southeast Texas special issue of aerosol science and technologyon findings from the fine particulate matter supersites program [J]. *Aerosol Science and Technology*, 2004, **38**: 14-26.

[10] Hasheminassab S, Pakbin P, Delfino R J, *et al.* Diurnal and seasonal trends in the apparent density of ambient fine and coarse particles in Los Angeles [J]. *Environ Pollut*, 2014, **187**: 1-9.

[11] Pitz M, Schmid O, Heinrich J, *et al.* Seasonal and diurnal variation of $PM_{2.5}$ apparent particle density in urban air in Augsburg,Germany [J]. *Environmental Science &Technology*, 2008, **42**(14): 5087-5093.

[12] Jiao L, Xu G, Zhao S, *et al*. LUR-based simulation of the spatial distribution of $PM_{2.5}$ of Wuhan [J]. *Geomatics and Information Science of Wuhan University*, 2015, **40**(8): 1088- 1094(Ch).

[13] Hoek G, Beelen R, de Hoogh K, *et al*. A review of land-use regression models to assess spatial variation of outdoor air pollution [J]. *Atmospheric Environment*, 2008, **42**(33): 7561-7578.

[14] Zou B, Pu Q, Bilal M, *et al*. High-resolution satellite mapping of fine particulates based on geographically weighted regression [J]. *IEEE Geoscience and Remote Sensing Letters*, 2016, **13**(4): 495-499.

[15] Carrat F, Valleron A J. Epidemiologic mapping using the "Kriging" method: Application to an influenza-like epidemic in France [J]. *American Journal of Epidemiology*, 1992, **135**(11): 1293-1300.

[16] Zou B, Zhan F B, Zeng Y, *et al.* Performance of Kriging and EWPM for relative air pollution exposure risk assessment [J]. *International Journal of Environmental Research*, 2011, **5**(3): 769-778.

[17] Liu G, Bi R, Wang S, *et al.* The use of spatial autocorrelation analysis to identify PAHs pollution hotspots at an industrially contaminated site [J]. *Environ Monit Assess*, 2013, **185**(11): 9549-9558.

[18] Zhao X J, Zhang X L, Xu X F, *et al.* Seasonal and diurnal variations of ambient $PM_{2.5}$ concentration in urban and rural environments in Beijing [J]. *Atmospheric Environment*, 2009, **43**(18): 2893-2900.

[19] Hu J L,Wang Y G, Ying Q, *et al.* Spatial and temporal variability of $PM_{2.5}$ and PM_{10} over the North China Plain and the Yangtze River Delta, China [J]. *Atmospheric Environment*, 2014, **95**: 598-609.

[20] Tobler W R. A computer movie simulating urban growth in the Detroit region [J]. *Economic Geography*, 1970, **46**: 234-240.

[21] Moran P A P. Notes on continuous stochastic phenomena [J]. *Biometrika*, 1950, **37**(1/2): 17-23.

[22] Geary R C. The contiguity ratio and statistical mapping [J]. *The Incorporated Statistician*, 1954, **5**(3):115-146.

[23] Cliff A D. *Spatial processes*: *Models & applications* [M]. London: Pion, 1981.

[24] Anselin L. Local indicators of spatial association—LISA [J]. *Geographical Analysis*, 1995, **27**(2): 93-115.

[25] Ross Z, Jerrett M, Ito K, *et al.* A land use regression for predicting fine particulate matter concentrations in the New York City region [J]. *Atmospheric Environment*, 2007, **41**(11): 2255-2269.

[26] Matheron G. *The Theory of Regionalized Variables and Its Applications* [D]. Paris: École national supérieure des mines, 1971.

[27] Krige D. *A Statistical Approach to Some Mine Valuations and Allied Problems at the Witwatersrand* [D]. Witwatersrand: University of Witwatersrand, 1951.

[28] Bayraktar H, Turalioglu F S. A Kriging-based approach for locating a sampling site—In the assessment of air quality [J]. *Stochastic Environmental Research and Risk Assessment*, 2005, **19**(4): 301-305.

[29] Vicedo-Cabrera A M, Biggeri A, Grisotto L, *et al.* A Bayesian Kriging model for estimating residential exposure to air pollution of children living in a high-risk area in Italy [J]. *Geospatial Health*, 2013, **8**(1): 87-95.

[30] Liao D P, Peuquet D J, Duan Y K, *et al*. GIS approaches for the estimation of residential-level ambient PM concentrations [J]. *Environmental Health Perspectives*, 2006, **114**(9): 1374-1380.

[31] Lü C, Tian H. Spatial and temporal patterns of nitrogen deposition in China: Synthesis of observational data [J]. *Journal of Geophysical Research*, 2007, **112**: D22S05.

[32] Ma Z, Hu X, Huang L, *et al.* Estimating ground-level $PM_{2.5}$ in China using satellite remote sensing [J]. *Environ Sci Technol*, 2014, **48**(13): 7436-7444.

□